ACS OMEGA

Open Access

http://pubs.acs.org/journal/acsodf

Article

MXene Hybrid Nanosheet of WS_2/Ti_3C_2 for Electrocatalytic Hydrogen Evolution Reaction

Mahider Asmare Tekalgne,[‖] Ha Huu Do,[‖] Tuan Van Nguyen, Quyet Van Le, Sung Hyun Hong, Sang Hyun Ahn,* and Soo Young Kim*

Cite This: *ACS Omega* 2023, 8, 41802−41808

Read Online

ACCESS | Metrics & More | Article Recommendations | Supporting Information

ABSTRACT: Designing low-cost hybrid electrocatalysts for hydrogen production is of significant importance. Recently, MXene-based materials are being increasingly employed in energy storage devices owing to their layered structure and high electrical conductivity. In this study, we propose a facile hydrothermal strategy for producing WS_2/Ti_3C_2 nanosheets that function as electrocatalysts in the hydrogen evolution reaction (HER). WS_2 provides a high surface area and active sites for electrocatalytic activity, whereas MXene Ti_3C_2 facilitates charge transfer. As a result, the synthesized WS_2/Ti_3C_2 offers an increased surface area and exhibits an enhanced electrocatalytic activity in acidic media. The WS_2/Ti_3C_2 (10%) catalyst exhibited a low onset potential of −150 mV versus RHE for the HER and a low Tafel slope of ∼62 mV dec^{-1}. Moreover, WS_2/Ti_3C_2 (10%) exhibited a double-layer capacitance of 1.2 mF/cm^{-2}, which is 3 and 6 times greater than those of bare WS_2 and Ti_3C_2, respectively. This catalyst also maintained a steady catalytic activity for the HER for over 1000 cycles.

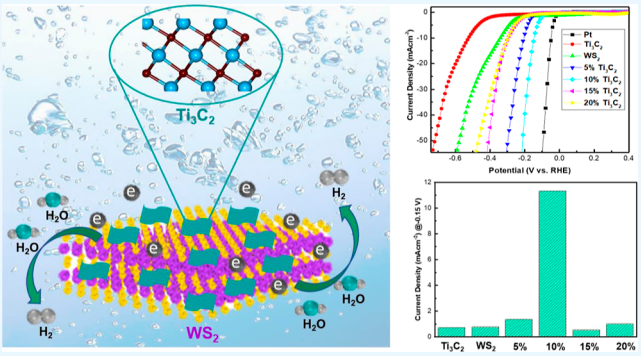

1. INTRODUCTION

To meet the rising demand for energy while reducing pollution, scientists have been studying the possibility of producing hydrogen from renewable sources such as water.[1−7] Electrochemical water splitting is one of the methods used for hydrogen production.[8−10] Several materials, such as graphene, carbon nanotubes,[11] metal carbides,[12,13] and transition metal dichalcogenides, were extensively investigated for replacing expensive noble-metal Pt-based materials in the hydrogen evolution reaction (HER).

Transition metal dichalcogenides (TMDs) exhibit unique properties in electrocatalytic HER, e.g., WS_2, a member of the TMD family, exhibits unique electronic properties and is widely studied owing to its low cost, high catalytic activity, and high stability.[14−21] Different methods were used to improve its electrical conductivity to widen its application such as cocatalyst loading, doping,[22] and heterostructure designing. For example, Hasani et al. investigated the effect of different metal dopants (Au, Ag, Pd, and Pt) on WS_2 for electrocatalytic hydrogen production.[23] The results showed that the Pd-doped WS_2 demonstrated an enhanced performance at a current density of 10 mA/cm^2 with low potentials of −175 and 54 mV dec^{-1}, respectively. This can be attributed to an energy band alignment caused by the presence of metal dopants. Moreover, other metal dopants also demonstrated an improved catalytic performance compared to bare WS_2. In another study, Jing et al. prepared and investigated a heterostructure of WS_2 and CoS_2 via hydrothermal and chemical vapor deposition (CVD) method.[24] The combination of these two materials improved the conductivity, owing to their tight connection; WS_2 helped in preventing the aggregation of CoS_2 nanoparticles, which subsequently increased the surface area. Consequently, the as-prepared sample showed a lower overpotential of 245 mV at 100 mA/cm^2 and a Tafel slope of 270 mV dec^{-1}. Therefore, developing an inexpensive and highly active cocatalyst is of paramount significance for achieving a higher performance in electrocatalytic H_2 production.

Recently, MXene, a new class of 2D materials, have garnered increasing attention owing to their excellent electrical conductivity[25−32] as well as high electrocatalytic activity in HER and have proven to be a potential substitute for expensive noble metal catalysts.[29,33−42] Recently, edge-oriented 1T-MoS_2 grown on modified Ti_3C_2[43] was prepared, and its HER performance was enhanced to a after being composited with Ti_3C_2. The advancement of MXene-based hybrid systems is in its infancy compared to other established 2D materials. However, MXene-based hybrids with interesting hierarchical

Received: August 28, 2023
Accepted: October 4, 2023
Published: October 23, 2023

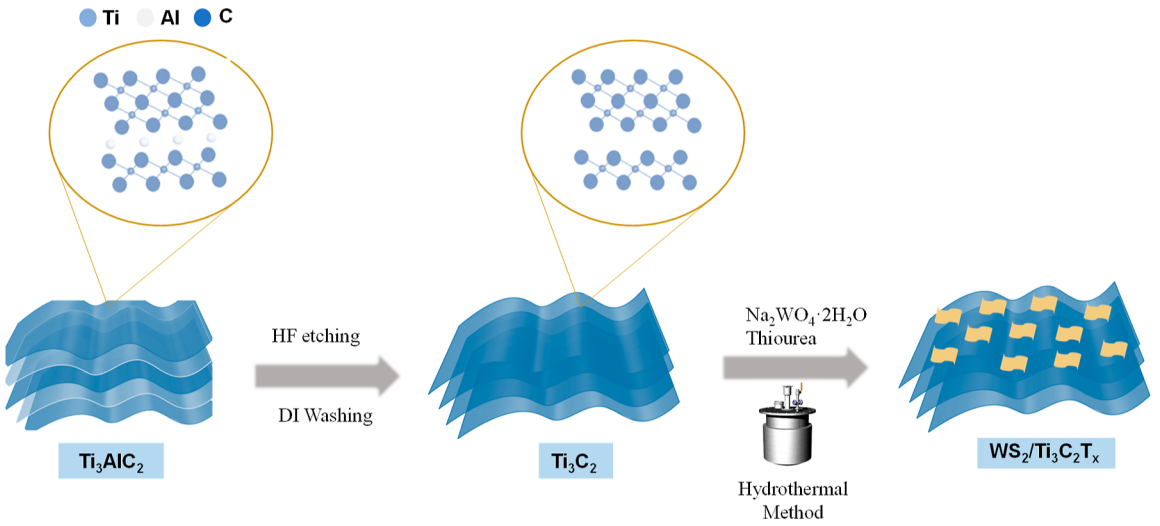

Figure 1. Schematic illustration of the synthesis process of WS_2/Ti_3C_2.

structures and excellent performance are attracting considerable interest.

In this work, a hybrid structure of WS_2 and Ti_3C_2 MXene for the HER is reported. A one-step hydrothermal method was used to synthesize WS_2/Ti_3C_2, where Ti_3C_2, MXene, and WS_2 play crucial roles in the reduction process, as shown in Figure 1. The electrochemical measurements of newly designed $WS_2/Ti_3C_2T_x$ (10%) exhibited better activity for HER than the other ratios used, such as 5, 15, and 20%. The sample had an improved onset potential and lower Tafel slope of 130 mv and 62 mV dec^{-1}, respectively. This enhancement is attributed to the larger surface area that resulted in a greater number of active sites and higher charge transfer. These results present an important pathway toward designing low-cost, efficient catalysts.

2. EXPERIMENTAL SECTION

2.1. Materials. Sodium tungstate dihydrate ($Na_2WO_4 \cdot 2H_2O$), thiourea, hydrochloric acid [HCl], Ti_3AlC_2 (MAX), and 5% Nafion solution were purchased from Sigma-Aldrich. Deionized (DI) water was obtained from Millipore Milli-Q at 18.3 MΩ·cm.

2.2. Ti_3C_2 MXene Synthesis. One gram portion of Ti_3AlC_2 MAX powder was mixed in 20 mL of hydrofluoric acid solution (48 wt %) and stirred for 48 h. Next, the mixed solution was washed with deionized (DI) water to neutrality. Lastly, Ti_3C_2 MXene was dried at 60 °C overnight in a vacuum oven.

2.3. WS_2/Ti_3C_2 Synthesis. A layered WS_2/Ti_3C_2 hybrid structure was synthesized by a one-step hydrothermal method. 0.4 mmol $Na_2WO_4 \cdot 2H_2O$, 2 mmol thiourea, and a Ti_3C_2 powder equal to 5%, 10%, 15%, or 20% by mass of $Na_2WO_4 \cdot 2H_2O$ were added to distilled water and stirred for 30 min at room temperature. Then, the as prepared solution was heated at 180 °C for 24 h in a 20 mL Teflon-lined autoclave. Then, the black precipitate was collected by centrifugation, washed three times with distilled water, and dried in a vacuum oven at 60 °C for 12 h.

2.4. Electrochemical Measurements. All electrochemical measurements were achieved on a standard three-electrode electrolytic system using an Ivium potentiostat V55630. The saturated calomel electrode (SCE) (reference), graphite rod (counter), and synthesized WS_2 on a glassy carbon electrode (working electrode) were used. The HER performance was calculated by linear sweep voltammetry (LSV) with a scan rate of 10 mV s^{-1} in 0.5 M H_2SO_4. An *iR* correction was also made. Continuous cyclic voltammograms at a scan rate of 50 mV s^{-1} were used to measure the stability of the prepared sample over 1000 cycles. Also, electrochemical impedance spectroscopy (EIS) was performed over a frequency range of 0.1 Hz−100 kHz. Reversible hydrogen electrode (RHE) potentials were used using the following equation

$$E(\mathrm{RHE}) = E(\mathrm{SCE}) + E_0(\mathrm{SCE}) + 0.059(\mathrm{pH})$$

2.5. Materials Characterization. The X-ray diffraction (XRD) spectra of the as-prepared samples were recorded using a powder X-ray diffractometer (Bruker New D8-Advance, Seoul, Korea) using Cu Kα radiation (λ = 0.154 nm). Raman spectra (Horiba, Japan) were recorded at an excitation wavelength of 514 nm. In addition, FE-SEM (Zeiss 300 VP) images were obtained at an acceleration voltage of 50 kV, and X-ray photoelectron spectroscopy (XPS, VG Scientific Ltd., England) was carried out under a vacuum greater than 1×10^{-5} mbar. Mg Kα radiation (1250 eV) was used with a constant pass energy of 50 eV.

3. RESULTS AND DISCUSSION

The crystal structures of the samples prepared in this work were evaluated by XRD. The XRD data of MAX phase Ti_3AlC_2 and HF etched Ti_3C_2 are shown in Figure S1. Glass substrate was used to measure the samples. The peak positions of Ti_3AlC_2 appearing at 2θ = 9.4, 33.8, and 38.9° were assigned to the (002), (101), and (104) faces, respectively. For Ti_3C_2, the peaks at 2θ = 33.8 and 38.9° and the other peaks disappeared because the Al atoms were eliminated by HF.[30] In addition, the peak at 9.4° in Ti_3AlC_2 is shifted to lower value of 5.9° in Ti_3C_2 MXene shown in Figure S1(a) and is broadened which results from the larger *d*-spacing explained by the expansion of surface from etching of the Al layer. Also, the XRD peak for WS_2 and WS_2/Ti_3C_2 is provided in Figure S2(a). The Raman spectra of synthesized Ti_3C_2, WS_2, and WS_2/Ti_3C_2 (10%) were also recorded; the results are shown in Figure S1(b). The peaks appeared at 350 and 410 cm^{-1}, thereby confirming the formation of WS_2.

Field-emission scanning electron microscopy (FE-SEM) was used to analyze the morphology of the as-prepared structures as shown in Figure 2, which confirmed successful growth of layered

https://doi.org/10.1021/acsomega.3c06403
ACS Omega 2023, 8, 41802−41808

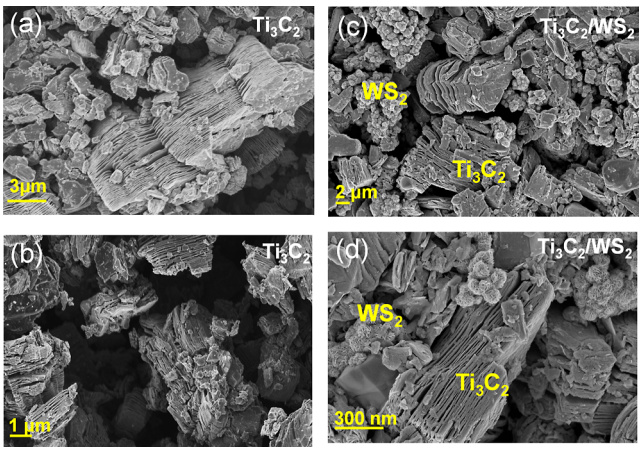

Figure 2. FE-SEM images: (a,b) Ti_3C_2 and (c,d) Ti_3C_2/WS_2.

structures of both Ti_3C_2 and WS_2. The pristine WS_2 showed a nanosheet like structure, as shown in Figure S2. After the HF etching process, loosely stacked nanosheets of Ti_3C_2 were generated thereby confirming the efficient removal of the interlayer aluminum in Ti_3AlC_2. The obtained Ti_3C_2 exhibited an accordion-like multilayer structure with a flat surface and an opened interspace, as shown in Figure 2a,b. In Figure 2c,d, the images of hybrid structure WS_2/Ti_3C_2 (10%) are shown. In addition, the FESEM images for WS_2/Ti_3C_2 (5%) and WS_2/Ti_3C_2 (15%) are shown in Figure S3. The resulting intimate hybrid structure of WS_2/Ti_3C_2 allowed direct charge transfer between WS_2 and Ti_3C_2, enhancing the electrocatalytic performance.

In addition, transmission electron microscopy (TEM) images of WS_2/Ti_3C_2 were obtained. Figure 3a,b show a general TEM image of the prepared WS_2/Ti_3C_2 sample. The Ti_3C_2 and WS_2 nanosheets were closely packed onto the surface of the structure. This structure allows a better electrical transfer resulting in the enhancement of HER catalytic performance. The TEM image in Figure 3c shows that the WS_2 nanosheets are interrelated with each other. As shown in Figure 3d, the elements W, S, Ti, and C were well distributed over the whole structure.

X-ray photoelectron spectroscopy (XPS) analyses were conducted on the WS_2/Ti_3C_2 catalysts to elucidate their valence states and chemical compositions. The XPS images of various WS_2/Ti_3C_2 samples indicated the presence of W, S, Ti, C, and O. Moreover, all of the prepared samples were analyzed via XPS, as shown in Figure 4, and full surveys of the W 4f and S 2p spectra of the WS_2 samples were obtained. Figure 4a shows a typical XPS survey spectrum of the WS_2/Ti_3C_2 samples, demonstrating that the samples are composed of the elements W, S, Ti, C, and O. Compared to the pristine WS_2 Figure S4 the high-resolution W $4f_{5/2}$ and W $4f_{7/2}$ spectra of the sample WS_2/Ti_3C_2 (10%) were positioned at 32.2 and 34.3 eV, with a shift of 0.7 and 0.4 eV, respectively, as shown in Figure 4b confirming the successful combination of WS_2 and Ti_3C_2. The S $2p_{3/2}$ and S $2p_{1/2}$ peaks were positioned at 161 and 162.5 eV, respectively. High-resolution XPS spectra of Ti 2p and C 1s are shown in Figure 4c,d, respectively. The Ti $2p_{3/2}$ and Ti $2p_{1/2}$ components located at approximately 455.3 and 461.5 eV, respectively, corresponded to Ti−C bonds.[31]

In addition, the Ti $2p_{3/2}$ and Ti $2p_{1/2}$ of Ti−O bonds are located at 458.7 and 464.4 eV, respectively. The C 1s core level can be fitted at 284.7, which belongs to the C−C bond, as shown in Figure 4c. XPS spectra of the WS_2/Ti_3C_2 (5%) and (15%) samples are also provided in Figures S5 and S6.

Electrocatalytic measurement was applied to measure the HER performance using a three-electrode configuration in 0.5 M H_2SO_4 acidic electrolyte solution. Glassy carbon electrode was used to load the prepared samples. The commercial Pt/C catalyst was used as a reference catalyst for the other catalysts as it has a small onset potential close to zero. The as-prepared WS_2/Ti_3C_2 samples were examined as electrocatalysts for the HER using a typical three-electrode system in the presence of a 0.5 M H_2SO_4 electrolyte solution. The 10% WS_2/Ti_3C_2 sample had a small overpotential of −150 mV with a Tafel slope of 62 mV dec^{-1} Figure 5a with Pt being the best sample.[44] Meanwhile, the 5, 15, and 20% WS_2/Ti_3C_2 samples also showed improved onset potentials of −210, −280, and −290 mV, respectively. In addition, the current density at 150 mV of all samples is given in Figure S9. Furthermore, the Tafel slopes also showed a similar trend. The pristine Ti_3C_2 had the highest Tafel slope of 132 mV dec^{-1} confirming its poor performance with regard to HER. Figure 5b shows the values of the Tafel slope, which are 73, 62, 84.2, and 85.5 mV dec^{-1} for the 5, 10, 15, and 20% cases, respectively; all of these are lower than that of WS_2, which has a slope of 88 mV dec^{-1}. These results demonstrate the enhanced performance of the hybrid structures that have abundant surface areas and active sites for the reduction process. Comparison of

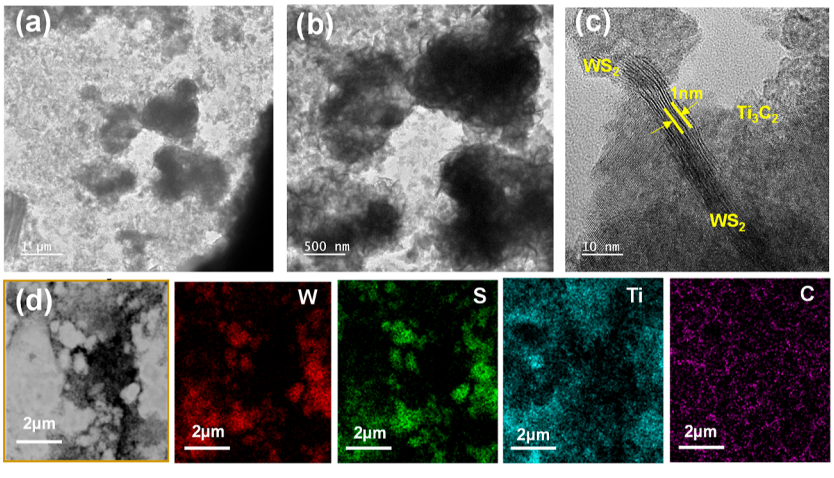

Figure 3. (a,b) TEM images at different magnifications, (c) HR-TEM and (d) EDX mapping of 10% Ti_3C_2/WS_2.

https://doi.org/10.1021/acsomega.3c06403
ACS Omega 2023, 8, 41802−41808

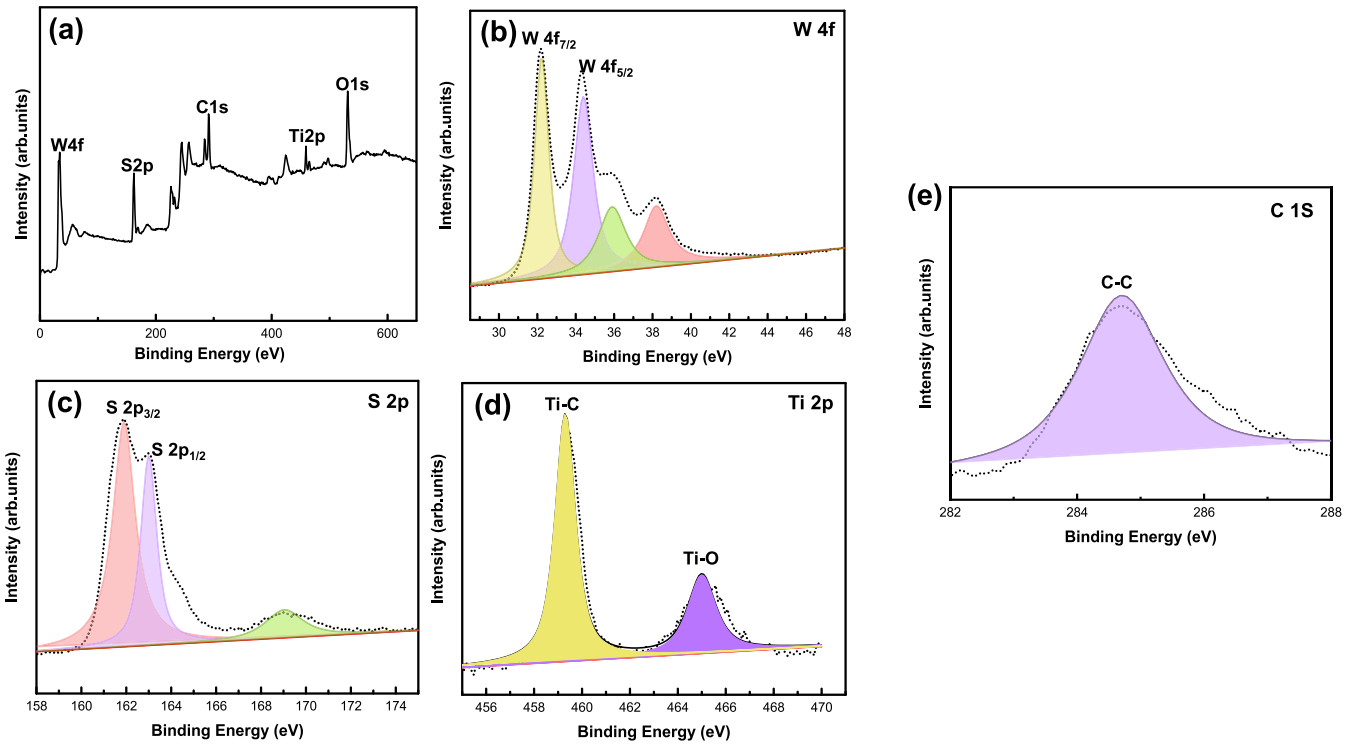

Figure 4. XPS spectra of WS_2/Ti_3C_2 (10%): (a) survey, (b) W 4f, (c) S 2p, (d) Ti 2p, and (e) C 1s.

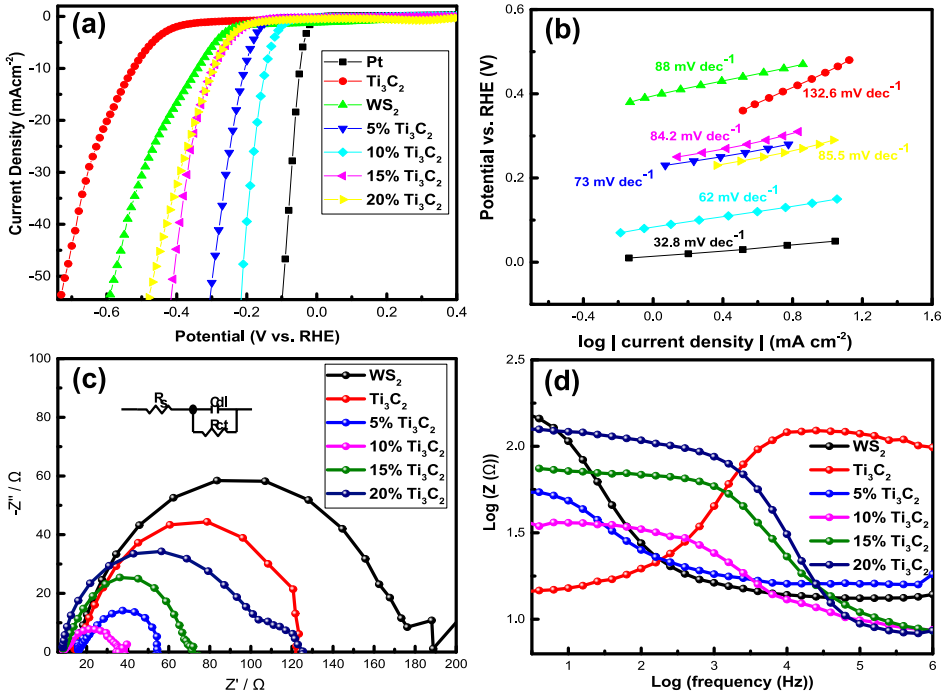

Figure 5. Electrochemical analysis of HER: (a) polarization curve of Pt, WS_2, and WS_2/Ti_3C_2 (5, 10, 15, and 20%, respectively); (b) Tafel slope of materials; (c) EIS Nyquist plot of materials; and (d) Bode plot of the samples.

the prepared sample with other similar reported catalysts is summarized in Table S2.

To investigate the kinetics between the prepared sample on the electrode and the electrolyte solution, we conducted EIS analysis was conducted. As a result, the charge transfer resistance (R_{ct}) value of the 10% $WS_2-Ti_3C_2$ MXene is found to be much smaller than that of WS_2/Ti_3C_2 or WS_2, as shown in Figure 5c; this confirms the remarkable electron transport capability of the 10% $WS_2-Ti_3C_2$ MXene. The WS_2 and Ti_3C_2 samples exhibited resistances of 190 and 120 Ω, respectively. WS_2/Ti_3C_2 (10%) showed a low R_{ct} (40 Ω), which is lower than that of the other three samples (55 Ω for 5%, 70 Ω for 15%, and 120 Ω for 20%) confirming a close interaction between Ti_3C_2 and WS_2 and enhancing the electron transfer in the electrocatalytic process. The corresponding Bode magnitude plot with respect to the phase frequency is presented in Figure 5d.

https://doi.org/10.1021/acsomega.3c06403
ACS Omega 2023, 8, 41802−41808

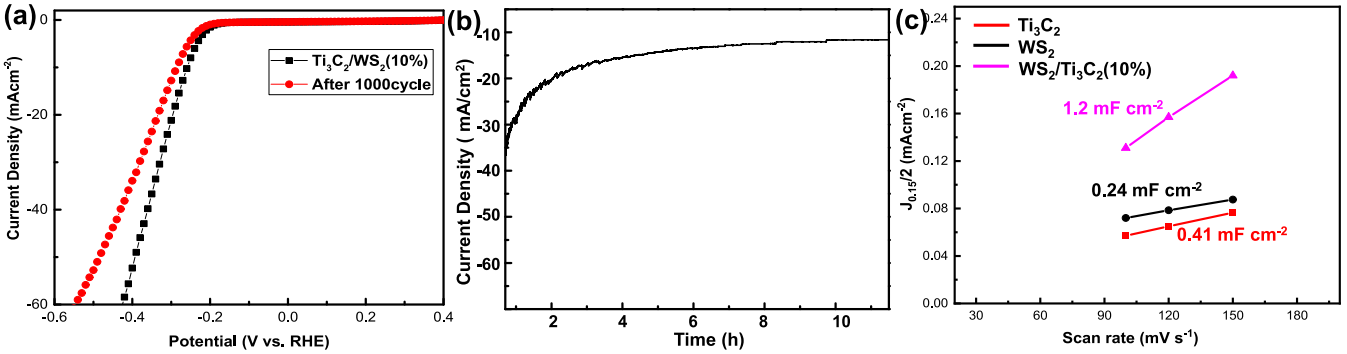

Figure 6. (a) Polarization curves were obtained initially and after 1000 cycles, and (b) time responses ($i-t$) recorded for 10 h (c) estimation of double-layer capacitance of the catalysts WS_2, Ti_3C_2, and WS_2/Ti_3C_2.

In addition, another effective criterion that should be used to evaluate a catalyst is its long-time stability. Long-term cycling tests of WS_2/Ti_3C_2 (10%) were conducted for 1000 cycles in an acidic media. As shown in Figure 6a, the sample does not show much difference before and after cycling, indicating that the WS_2/Ti_3C_2 (10%) catalyst displays excellent HER activity with long-term stability. The enhanced catalytic performance of WS_2/Ti_3C_2 (10%) can be attributed to two factors. First, the high conductivity of Ti_3C_2 enables fast charge transfer with its strong interaction with WS_2; and second, the number of active sites is increased, allowing a faster reduction of adsorbed hydrogen ions. In addition, a chronoamperometric study was conducted using a fixed current density of 10 mA/cm^2 to investigate the stability of WS_2/Ti_3C_2 (10%). Owing to its superior catalytic durability in acidic environments, WS_2/Ti_3C_2 (10%) showed a small decrease in current density and stable performance even after 10 h Figure 6c. Furthermore, the electrochemical surface area of the prepared samples was measured via double-layer capacitance (C_{dl}). Cyclic voltammetry curves (CVs) at scan rates of 20−150 mV s^{-1} were used to measure the values of C_{dl}. Figure S8 shows typical CV data for WS_2, Ti_3C_2, and $WS_2-Ti_3C_2$ at different ratios at different scan rates in an acidic medium. The C_{dl} of 10% WS_2 significantly increased from 0.41 to 1.2 mF/cm^2 WS_2/Ti_3C_2 (10%) after being coupled with Ti_3C_2 nanosheets, even though the C_{dl} of the Ti_3C_2 nanosheets was only 0.24 mF/cm^2, as shown in Figure 6b.

The mechanism of the WS_2/Ti_3C_2 MXene is shown in Figure 7. The metallic and highly conductive Ti_3C_2 promotes charge transfer and accelerates the kinetics of the HER. This is critical to achieve improved electrocatalytic performance. However, an optimum amount of Ti_3C_2 is necessary to achieve this enhanced result, as shown in the $I-V$ curve of Figure 5a. As shown in the potential curve in Figure 5a, the electrocatalytic activity improves and subsequently decreases as the concentration of the catalyst changes from 10 to 15%, as clearly shown by the change in trend of overpotentials upon catalyst loading, Table S1. As the amount of Ti_3C_2 increases, the surface of WS_2 will be covered and have fewer active sites for the adsorption of H^+ ions. Simultaneously, due to inadequate exposed sites of WS_2, and large R_{ct} on the electrode, the catalytic performance decreases as the concentration increases. Thus, a moderate amount of Ti_3C_2 is essential to attain the optimal catalytic activity for potential and possesses the synergistic effect of both materials. We believe that these hybrid-structured WS_2/Ti_3C_2 nanosheets are good alternatives for highly enhanced electrocatalytic hydrogen production.

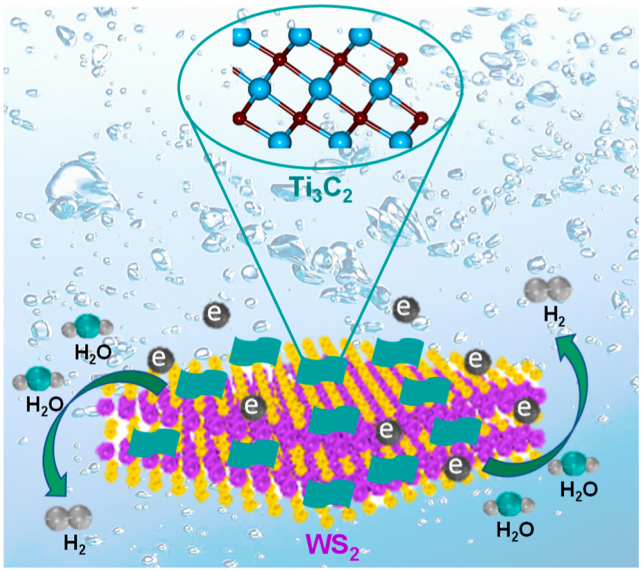

Figure 7. Schematic representation of the mechanism whereby 10% WS_2/Ti_3C_2 achieves electrochemical water splitting.

4. CONCLUSIONS

In conclusion, we synthesized an inexpensive WS_2/Ti_3C_2 hybrid structure for HER. The as-prepared samples with varied Ti_3C_2 to WS_2 mass ratios show enhanced catalytic performance than individual WS_2 and Ti_3C_2 nanosheets. The WS_2/Ti_3C_2 (10%) sample has the lowest overpotential of 150 mV and a Tafel slope of 62 mV dec^{-1}. The Improved electrocatalytic performance of the WS_2/Ti_3C_2 is credited to (1) the large surface area, and (2) rapid charge transfers due to the presence of Ti_3C_2 and its strong interaction to WS_2. The stability of WS_2/Ti_3C_2 (10%) in an acidic solution after 1000 cycles was also demonstrated.

■ ASSOCIATED CONTENT

Supporting Information

The Supporting Information is available free of charge at https://pubs.acs.org/doi/10.1021/acsomega.3c06403.

XRD patterns, Raman, FESEM images, XPS spectra, and electrochemical characterization results for the Ti_3AlC_2, Ti_3C_2, WS_2, and WS_2/Ti_3C_2; XRD and Raman spectra of Ti_3AlC_2, Ti_3C_2, and WS_2/Ti_3C_2; FESEM images of WS_2 at different magnifications; FESEM images of 5 and 15% Ti_3C_2/WS_2 at different magnifications; XPS spectra of the WS_2; XPS spectra of the WS_2/Ti_3C_2 (5%); XPS spectra of the WS_2/Ti_3C_2 (15%); atomic ratio comparison for

https://doi.org/10.1021/acsomega.3c06403
ACS Omega 2023, 8, 41802−41808

Ti_3C_2, 5, 10, and 15 WS_2/Ti_3C_2; cyclic voltammograms (0.1−0.2 V) of Ti_3C_2, WS_2, 5% Ti_3C_2, 10% Ti_3C_2, 15% Ti_3C_2, and 20% Ti_3C_2 at different scan rates (20−150 mV s^{-1}); current density comparison @150 mV for Ti_3C_2, WS_2, and 5, 10, 15, and 20% WS_2/Ti_3C_2; comparison of the overpotential, onset potential, and Tafel slope for different samples; and comparison of overpotential at 10 mA/cm^2 and Tafel slopes from other reports (PDF)

AUTHOR INFORMATION

Corresponding Authors

Sang Hyun Ahn − *School of Chemical Engineering and Materials Science, Chung-Ang University, Seoul 06974, Republic of Korea;* orcid.org/0000-0001-8906-5908; Email: shahn@cau.ac.kr

Soo Young Kim − *Department of Materials Science and Engineering, Institute of Green Manufacturing Technology, Korea University, Seoul 02841, Republic of Korea;* orcid.org/0000-0002-0685-7991; Email: sooyoungkim@korea.ac.kr

Authors

Mahider Asmare Tekalgne − *Department of Materials Science and Engineering, Institute of Green Manufacturing Technology, Korea University, Seoul 02841, Republic of Korea*

Ha Huu Do − *VKTech Research Center, NTT Hi-Tech Institute, Nguyen Tat Thanh University, Ho Chi Minh City 700000, Vietnam*

Tuan Van Nguyen − *Department of Materials Science and Engineering, Institute of Green Manufacturing Technology, Korea University, Seoul 02841, Republic of Korea*

Quyet Van Le − *Department of Materials Science and Engineering, Institute of Green Manufacturing Technology, Korea University, Seoul 02841, Republic of Korea*

Sung Hyun Hong − *Department of Materials Science and Engineering, Institute of Green Manufacturing Technology, Korea University, Seoul 02841, Republic of Korea*

Complete contact information is available at: https://pubs.acs.org/10.1021/acsomega.3c06403

Author Contributions

‖M.A.T. and H.H.D. contributed equally.

Notes

The authors declare no competing financial interest.

ACKNOWLEDGMENTS

This work was supported by the National Research Foundation of Korea (NRF) funded by the Korean government (2021R1A4A3027878 and 2022M3H4A1A01012712).

REFERENCES

(1) Cabán-Acevedo, M.; Stone, M. L.; Schmidt, J.; Thomas, J. G.; Ding, Q.; Chang, H.-C.; Tsai, M.-L.; He, J.-H.; Jin, S. Efficient Hydrogen Evolution Catalysis Using Ternary Pyrite-Type Cobalt Phosphosulphide. *Nat. Mater.* **2015**, *14*, 1245−1251.

(2) Zheng, Y.; Jiao, Y.; Zhu, Y.; Li, L. H.; Han, Y.; Chen, Y.; Du, A.; Jaroniec, M.; Qiao, S. Z. Hydrogen Evolution by a Metal-Free Electrocatalyst. *Nature* **2014**, *5*, 3783.

(3) Wang, Q.; Mi, F.; Li, J.; Wu, Y.; Zhou, X.; Ma, G.; Ren, S. Tungsten Doping Generated Mo_2C-MoC Heterostructure to Improve Her Performance in Alkaline Solution. *Electrochim. Acta* **2021**, *370*, 137796.

(4) Dresselhaus, M.; Thomas, I. L. Alternative Energy Technologies. *Nature* **2001**, *414*, 332−337.

(5) Turner, J. A. Sustainable Hydrogen Production. *Energy Fuels* **2004**, *305*, 972−974.

(6) Chen, Z.; Duan, X.; Wei, W.; Wang, S.; Ni, B.-J. Recent Advances in Transition Metal-Based Electrocatalysts for Alkaline Hydrogen Evolution. *J. Mater. Chem. A* **2019**, *7*, 14971−15005.

(7) You, B.; Tang, M. T.; Tsai, C.; Abild-Pedersen, F.; Zheng, X.; Li, H. Enhancing Electrocatalytic Water Splitting by Strain Engineering. *Adv. Mater.* **2019**, *31*, 1807001.

(8) Ouyang, T.; Ye, Y. Q.; Wu, C. Y.; Xiao, K.; Liu, Z. Q. Heterostructures Composed of N-Doped Carbon Nanotubes Encapsulating Cobalt and B-Mo_2C Nanoparticles as Bifunctional Electrodes for Water Splitting. *Angew. Chem.* **2019**, *131*, 4977−4982.

(9) Kuang, P.; Tong, T.; Fan, K.; Yu, J. In Situ Fabrication of Ni-Mo Bimetal Sulfide Hybrid as an Efficient Electrocatalyst for Hydrogen Evolution over a Wide Ph Range. *ACS Catal.* **2017**, *7*, 6179−6187.

(10) Kuang, P.; He, M.; Zou, H.; Yu, J.; Fan, K. 0d/3d MoS_2-NiS_2/N-Doped Graphene Foam Composite for Efficient Overall Water Splitting. *Appl. Catal., B* **2019**, *254*, 15−25.

(11) Lee, S.-H.; Park, J. H.; Kim, S. M. Synthesis, Property, and Application of Carbon Nanotube Fiber. *J. Korean Ceram. Soc.* **2021**, *58*, 148−159.

(12) Vrubel, H.; Hu, X. Molybdenum Boride and Carbide Catalyze Hydrogen Evolution in Both Acidic and Basic Solutions. *Angew. Chem., Int. Ed.* **2012**, *51*, 12703−12706.

(13) Chen, W.-F.; Wang, C.-H.; Sasaki, K.; Marinkovic, N.; Xu, W.; Muckerman, J. T.; Zhu, Y.; Adzic, R. R. Highly Active and Durable Nanostructured Molybdenum Carbide Electrocatalysts for Hydrogen Production. *Energy Environ. Sci.* **2013**, *6*, 943−951.

(14) Han, G.-Q.; Liu, Y.-R.; Hu, W.-H.; Dong, B.; Li, X.; Chai, Y.-M.; Liu, Y.-Q.; Liu, C.-G. WS_2 Nanosheets Based on Liquid Exfoliation as Effective Electrocatalysts for Hydrogen Evolution Reaction. *Mater. Chem. Phys.* **2015**, *167*, 271−277.

(15) Tong, R.; Qu, Y.; Zhu, Q.; Wang, X.; Lu, Y.; Wang, S.; Pan, H. Combined Experimental and Theoretical Assessment of WX_y (X= C, N, S, P) for Hydrogen Evolution Reaction. *ACS Appl. Energy Mater.* **2020**, *3*, 1082−1088.

(16) Yan, H.; Tian, C.; Wang, L.; Wu, A.; Meng, M.; Zhao, L.; Fu, H. Phosphorus-Modified Tungsten Nitride/Reduced Graphene Oxide as a High-Performance, Non-Noble-Metal Electrocatalyst for the Hydrogen Evolution Reaction. *Angew. Chem.* **2015**, *127*, 6423−6427.

(17) Holt, C. M.; Murphy, S.; Gray, M. R.; Mitlin, D. Electrocatalytic Hydrogenation of 2-Cyclohexen-1-One in a High Sulfur Environment Using a Carbon-Supported Nanostructured Tungsten Sulfide Catalyst. *Catal. Commun.* **2010**, *12*, 314−317.

(18) Wang, F.; Shifa, T. A.; Zhan, X.; Huang, Y.; Liu, K.; Cheng, Z.; Jiang, C.; He, J. Recent Advances in Transition-Metal Dichalcogenide Based Nanomaterials for Water Splitting. *Nanoscale* **2015**, *7*, 19764−19788.

(19) Yang, J.; Shin, H. S. Recent Advances in Layered Transition Metal Dichalcogenides for Hydrogen Evolution Reaction. *J. Mater. Chem. A* **2014**, *2*, 5979−5985.

(20) Nguyen, T. P.; Nguyen, D. L. T.; Nguyen, V.-H.; Le, T.-H.; Ly, Q. V.; Vo, D.-V. N.; Nguyen, Q. V.; Le, H. S.; Jang, H. W.; Kim, S. Y.; et al. Facile Synthesis of WS_2 Hollow Spheres and Their Hydrogen Evolution Reaction Performance. *Appl. Surf. Sci.* **2020**, *505*, 144574.

(21) Jung, Y.; Ji, E.; Capasso, A.; Lee, G.-H. Recent Progresses in the Growth of Two-Dimensional Transition Metal Dichalcogenides. *J. Korean Ceram. Soc.* **2019**, *56*, 24−36.

(22) Jiang, A.; Zhang, B.; Li, Z.; Jin, G.; Hao, J. Vanadium-Doped WS_2 Nanosheets Grown on Carbon Cloth as a Highly Efficient Electrocatalyst for the Hydrogen Evolution Reaction. *Chemistry - An Asian Journal* **2018**, *13*, 1438−1446.

(23) Hasani, A.; Nguyen, T. P.; Tekalgne, M.; Van Le, Q.; Choi, K. S.; Lee, T. H.; Jung Park, T.; Jang, H. W.; Kim, S. Y. The Role of Metal Dopants in WS_2 Nanoflowers in Enhancing the Hydrogen Evolution Reaction. *Appl. Catal., A* **2018**, *567*, 73−79.

(24) Jing, Y.; Mu, X.; Xie, C.; Liu, H.; Yan, R.; Dai, H.; Liu, C.; Zhang, X.-D. Enhanced Hydrogen Evolution Reaction of WS_2-CoS_2

Heterostructure by Synergistic Effect. *Int. J. Hydrog. Energy.* **2019**, *44*, 809−818.
(25) Anasori, B.; Lukatskaya, M. R.; Gogotsi, Y. 2D Metal Carbides and Nitrides (MXenes) for Energy Storage. *Nat. Rev. Mater.* **2017**, *2*, 16098.
(26) Lukatskaya, M. R.; Mashtalir, O.; Ren, C. E.; Dall'Agnese, Y.; Rozier, P.; Taberna, P. L.; Naguib, M.; Simon, P.; Barsoum, M. W.; Gogotsi, Y. Cation Intercalation and High Volumetric Capacitance of Two-Dimensional Titanium Carbide. *Nat. Commun.* **2013**, *341*, 1502−1505.
(27) Ghidiu, M.; Lukatskaya, M. R.; Zhao, M.-Q.; Gogotsi, Y.; Barsoum, M. W. Conductive Two-Dimensional Titanium Carbide 'Clay'with High Volumetric Capacitance. *Nature* **2014**, *516*, 78−81.
(28) Lipatov, A.; Lu, H.; Alhabeb, M.; Anasori, B.; Gruverman, A.; Gogotsi, Y.; Sinitskii, A. Elastic Properties of 2d $Ti_3C_2T_x$ Mxene Monolayers and Bilayers. *Sci. Adv.* **2018**, *4*, No. eaat0491.
(29) Gao, G.; O'Mullane, A. P.; Du, A. 2D MXenes: A New Family of Promising Catalysts for the Hydrogen Evolution Reaction. *ACS Catal.* **2017**, *7*, 494−500.
(30) Naguib, M.; Kurtoglu, M.; Presser, V.; Lu, J.; Niu, J.; Heon, M.; Hultman, L.; Gogotsi, Y.; Barsoum, M. W. Two-Dimensional Nanocrystals Produced by Exfoliation of Ti_3AlC_2. *Adv. Mater.* **2011**, *23*, 4248−4253.
(31) Yoon, Y.; Lee, M.; Kim, S. K.; Bae, G.; Song, W.; Myung, S.; Lim, J.; Lee, S. S.; Zyung, T.; An, K. S. A Strategy for Synthesis of Carbon Nitride Induced Chemically Doped 2d Mxene for High-Performance Supercapacitor Electrodes. *Adv. Energy Mater.* **2018**, *8*, 1703173.
(32) Yan, J.; Ren, C. E.; Maleski, K.; Hatter, C. B.; Anasori, B.; Urbankowski, P.; Sarycheva, A.; Gogotsi, Y. Flexible Mxene/Graphene Films for Ultrafast Supercapacitors with Outstanding Volumetric Capacitance. *Adv. Funct. Mater.* **2017**, *27*, 1701264.
(33) Ling, C.; Shi, L.; Ouyang, Y.; Wang, J. Searching for Highly Active Catalysts for Hydrogen Evolution Reaction Based on O-Terminated Mxenes through a Simple Descriptor. *Chem. Mater.* **2016**, *28*, 9026−9032.
(34) Seh, Z. W.; Fredrickson, K. D.; Anasori, B.; Kibsgaard, J.; Strickler, A. L.; Lukatskaya, M. R.; Gogotsi, Y.; Jaramillo, T. F.; Vojvodic, A. Two-Dimensional Molybdenum Carbide (MXene) as an Efficient Electrocatalyst for Hydrogen Evolution. *ACS Energy Lett.* **2016**, *1*, 589−594.
(35) Zhou, S.; Yang, X.; Pei, W.; Liu, N.; Zhao, J. Heterostructures of MXenes and N-Doped Graphene as Highly Active Bifunctional Electrocatalysts. *Nanoscale* **2018**, *10*, 10876−10883.
(36) Li, P.; Zhu, J.; Handoko, A. D.; Zhang, R.; Wang, H.; Legut, D.; Wen, X.; Fu, Z.; Seh, Z. W.; Zhang, Q. High-Throughput Theoretical Optimization of the Hydrogen Evolution Reaction on Mxenes by Transition Metal Modification. *J. Mater. Chem. A* **2018**, *6*, 4271−4278.
(37) Guo, Z.; Zhou, J.; Sun, Z. New Two-Dimensional Transition Metal Borides for Li Ion Batteries and Electrocatalysis. *J. Mater. Chem. A* **2017**, *5*, 23530−23535.
(38) Handoko, A. D.; Fredrickson, K. D.; Anasori, B.; Convey, K. W.; Johnson, L. R.; Gogotsi, Y.; Vojvodic, A.; Seh, Z. W. Tuning the Basal Plane Functionalization of Two-Dimensional Metal Carbides (MXenes) to Control Hydrogen Evolution Activity. *ACS Appl. Energy Mater.* **2018**, *1*, 173−180.
(39) Pandey, M.; Thygesen, K. S. Two-Dimensional Mxenes as Catalysts for Electrochemical Hydrogen Evolution: A Computational Screening Study. *J. Phys. Chem. C* **2017**, *121*, 13593−13598.
(40) Pan, H. Ultra-High Electrochemical Catalytic Activity of Mxenes. *Nature* **2016**, *6*, 32531.
(41) Li, S.; Tuo, P.; Xie, J.; Zhang, X.; Xu, J.; Bao, J.; Pan, B.; Xie, Y. Ultrathin Mxene Nanosheets with Rich Fluorine Termination Groups Realizing Efficient Electrocatalytic Hydrogen Evolution. *Nano energy* **2018**, *47*, 512−518.
(42) Jiang, W.; Zou, X.; Du, H.; Gan, L.; Xu, C.; Kang, F.; Duan, W.; Li, J. Universal Descriptor for Large-Scale Screening of High-Performance Mxene-Based Materials for Energy Storage and Conversion. *Chem. Mater.* **2018**, *30*, 2687−2693.
(43) Li, X.; Lv, X.; Sun, X.; Yang, C.; Zheng, Y.-Z.; Yang, L.; Li, S.; Tao, X. Edge-Oriented, High-Percentage 1t′-Phase MoS_2 Nanosheets Stabilize Ti_3C_2 Mxene for Efficient Electrocatalytic Hydrogen Evolution. *Appl. Catal., B* **2021**, *284*, 119708.
(44) Ai, L.; Su, J.; Wang, M.; Jiang, J. Bamboo-Structured Nitrogen-Doped Carbon Nanotube Coencapsulating Cobalt and Molybdenum Carbide Nanoparticles: An Efficient Bifunctional Electrocatalyst for Overall Water Splitting. *ACS Sustainable Chem. Eng.* **2018**, *6*, 9912−9920.

https://doi.org/10.1021/acsomega.3c06403
ACS Omega 2023, 8, 41802−41808